Multifunctional cosmetic potential of extracellular vesicle-like nanoparticles derived from the stem of *Cannabis sativa* in treating pigmentation disorders

HYEON JIN LEE[1,2], YUN HYE KIM[1,3], SEO JUN LEE[1], SU HYUN PARK[1], JAE-MIN YUK[2], JAE CHEOL JEONG[4], YOUNG BAE RYU[1] and WOO SIK KIM[1]

[1]Functional Biomaterial Research Center, Korea Research Institute of Bioscience and Biotechnology, Jeongeup, North Jeolla 56212, Republic of Korea; [2]Department of Medical Science, College of Medicine, Chungnam National University, Daejeon, South Chungcheong 35015, Republic of Korea; [3]Department of Food and Nutrition, Chungnam National University, Daejeon, South Chungcheong 34134, Republic of Korea; [4]Biological Resource Center, Korea Research Institute of Bioscience and Biotechnology, Jeongeup, North Jeolla 56212, Republic of Korea

Received November 25, 2024; Accepted March 4, 2025

DOI: 10.3892/mmr.2025.13512

Abstract. While natural products and synthetic chemicals are used in functional cosmetics, their potential side effects remain a concern. This has driven the need for safer and more effective agents to treat skin disorders. This has driven the need safer and more effective agents to treat skin disorders. Therefore, the present study aimed to explore the functional properties of *Cannabis sativa* stem-derived nanoparticles (CSS-NPs) and evaluate their potential as a cosmetic ingredient. Using nanoparticle analysis, CSS-NPs, with a mean diameter of ~120 nm exhibited notable resistance to external stress conditions, including pH fluctuation and enzymatic degradation by DNase, RNase and proteinase K. They also contained 48 distinct biochemical components. *In vitro* assays revealed that CSS-NPs significantly downregulated the expression of genes and proteins associated with melanin synthesis in mouse B16F10 melanoma cells under α-melanocyte stimulating hormone (α-MSH)-induced hyperpigmentation. These inhibitory effects were mediated by the activation of ERK and Akt signaling pathways. Furthermore, CSS-NPs improved the viability of α-MSH-treated B16F10 cells; this was accompanied by the upregulation of antioxidant-associated enzymes and a decrease in α-MSH-induced reactive oxygen species levels. Collectively, these findings suggested that CSS-NPs carry out a key role in mitigating skin pigmentation and enhancing antioxidant defenses by modulating the ERK/Akt axis during excessive melanin synthesis. Thus, CSS-NPs represent a promising multifunctional cosmetic ingredient with potential in treating pigmentation disorders and protecting skin cells.

Correspondence to: Dr Young Bae Ryu or Dr Woo Sik Kim, Functional Biomaterial Research Center, Korea Research Institute of Bioscience and Biotechnology, 181 Ipsin-gil, Jeongeup, Jeollabuk 56212, Republic of Korea
E-mail: ybryu@kribb.re.kr
E-mail: kws6144@kribb.re.kr

Abbreviations: EV, extracellular vesicle; ROS, reactive oxygen species; CSS-NP, *Cannabis sativa* stem-derived EV-like nanoparticle; TFF, tangential flow filtration; SEM, scanning electron microscopy; Q-TOF-MS, quadrupole time-of-flight mass spectrometry; UPLC, ultra-high-performance liquid chromatography; GC, gas chromatography; α-MSH, α-melanocyte stimulating hormone; TYR, tyrosinase; DPPH, 2,2-diphenyl-1-picrylhydrazyl; ABTS, 2,2'-azino-bis(3-ethylbenzothiazoline-6-sulfonic acid) diammonium; TAC, total antioxidant capacity; CAT, catalase; MITF, microphthalmia-associated transcription factor; TRP, tyrosinase-related protein

Key words: Cannabis sativa, plant-derived nanoparticle, anti-melanogenic effect, antioxidant activity, melanocyte stimulating hormone, melanin, pigmentation disorder

Introduction

Melanin, synthesized within the melanosomes of melanocytes, serves a key role in determining skin pigmentation (1). In the epidermis, melanin is transferred to adjacent keratinocytes, where it serves as a protective barrier against ultraviolet radiation damage (2). However, abnormal melanin production can lead to pigmentary disorders, such as melasma, hyperpigmentation, freckles and vitiligo (3). While agents such as arbutin, kojic acid and hydroquinone are employed to treat these disorders, their efficacy is typically limited owing to poor skin penetration and absorption (4). Moreover, these agents are associated with side effects, including dryness, inflammation and a potentially increased risk of cancer (5,6). Some agents, such as hydroquinone, have been banned or restricted in certain countries owing to their potential health risks, further highlighting the limitations of current treatments (7). Therefore, there is a need for the development of efficient and safe transdermal agents and research has increasingly focused on using natural substances with fewer side effects for treating skin disease (5-7).

Plant-derived extracellular vesicles (EVs) sourced from edible plants, such as vegetables and fruits, are rich in bioactive molecules, including nucleic acid, protein, lipid and metabolites (8). These vesicles, ranging in size from 50 to 1,000 nm, have potential as therapeutic agents for various diseases because of their biocompatibility, safety and high functional efficiency (9,10). For example, EVs isolated from grapes, grapefruit and carrots have demonstrated anti-inflammatory properties in the treatment of severe inflammatory bowel disease (11-13). Additionally, ginseng root-derived EVs exhibit protective and anti-aging effects on cells damaged by ultraviolet B radiation, effectively reducing reactive oxygen species (ROS), decreasing cell mortality and mitigating oxidative stress responses (14). Notably, these plant-derived EVs are non-pathogenic and cost-effective to produce compared with mammalian counterparts (15). Moreover, they contain bioactive molecules, such as phytochemicals, which are beneficial to human health, making them promising candidates for treating or alleviating numerous diseases (16-18).

Cannabis sativa, commonly referred to as hemp, is one of the oldest medicinal plants and is also used in textiles (19). *Cannabis* extracts can carry out various biological activities, including antioxidant, anticancer and anti-inflammatory effects; however, previous studies have focused on seeds or leaves, limiting the research scope (20-23). Therefore, the present study aimed to explore the potential of *C. sativa* stem EV-like nanoparticles (CSS-NPs) as therapeutic agents or pharmaceuticals for treating skin disorders. Additionally, the present study aimed to investigate the cosmetic properties of CSS-NPs, particularly their whitening and antioxidant activity in melanoma cells, and to elucidate the underlying mechanism.

Materials and methods

Ethics approval. Experiments were conducted in compliance with the Narcotics Control Act of the Republic of Korea. The plant species used is not classified as protected or endangered.

Isolation of CSS-NPs. Stems of 2-month-old CS variety Cheungsam were collected in August 2022 from an open field at Jay Hemp Korea. Initially, stems were washed three times with sterile distilled water. After cutting into 2-cm pieces, 200 g CSS was mixed with 1 l PBS and ground in a mixer grinder at a 30-sec for a total of three cycles. The isolation of CSS-NPs involved centrifugation at 1,800, 3,500 and 10,000 x g for 20 min each at 4˚C. Supernatants were filtered using a 0.45-μm membrane filter (GVS S.p.A.). Filtered supernatants were first concentrated to a 15-ml using a tangential flow filtration (TFF) system equipped with a 500-kDa ultrafilter membrane (Pall Life Sciences). For purification, sucrose cushioned ultracentrifugation was performed using Optiprep solution (60% iodixanol; Stemcell Technologies). Specifically, 15 ml concentrated supernatant was transferred to a 17 ml ultracentrifuge tube (Beckman Coulter, Inc.) with 1 ml Optiprep using a Pasteur pipette (MilliporeSigma). The tubes were ultracentrifuged at 120,000 x g for 60 min at 4˚C (Optima XE-100; Beckman Coulter Inc.). The highly purified CSS-NPs were collected and dialyzed with 5 ml cold PBS. Finally, CSS-NPs were filtered using a 0.45-μm syringe filter (Advantec) and stored at -80˚C until further use. The protein concentration of CSS-NPs was determined using a BCA protein assay kit (Thermo Fisher Scientific, Inc.).

Physicochemical assessment of CSS-NPs. Size distribution and ζ potential of CSS-NPs were confirmed using qNano-Exoid (Izon Science Limited) according to the manufacturer's instructions using the NP200 nanopore (size; 85-500 nm). To visualize the morphology of CSS-NPs, scanning electron microscopy (SEM) was used. Samples were first mixed at 20˚C for 60 min with 4% paraformaldehyde solution for fixation. CSS-NPs were washed twice with PBS and dehydrated in 70% ethanol before the evaporation of ethanol. Following dehydration, the samples were coated with gold-palladium sputtering and assessed using a S-4700 scanning electron microscope (Hitachi, Ltd.). To evaluate the stability of CSS-NPs against external stimuli, CSS-NPs were exposed to different pH concentrations (pH 2.0 or 12.1) for 30 min at 37˚C. Additionally, CSS-NPs were incubated with 3 DNase (Thermo Fisher Scientific, Inc.), 6 RNase and 100 μg/ml proteinase K (both BioLabs) at 37˚C for 30 min, after which changes in size and ζ potential were measured.

Biochemical composition of CSS-NPs. Biochemical composition of CSS-NPs was evaluated using quadrupole time-of-flight mass spectrometry (Q-TOF-MS) and ultra-high-performance liquid chromatography (UPLC; both Waters Corporation). Briefly, 1 mg CSS-NPs was dried using a freezing/vacuum-drying system (VD-800F; TAITEC CORPORATION) and resuspended with 100 μl 80% methanol. UPLC was conducted by injecting 10 μl reconstituted sample onto an Acquity UPLC BEH C18 column (Waters Corporation). Q-TOF-MS and tandem MS spectra were acquired as previously described (24). For gas chromatography (GC)-MS analysis, 1 mg CSS-NPs were mixed with 70 μl hydroxymethyl amine solution, incubated at 37˚C for 90 min and then methylated with 70 μl N,O-bis(trimethylsilyl) trifluoroacetamide at 90˚C for 30 min. After cooling, 1.5 saturated NaCl solution and 1.0 ml n-hexane were added. Next, the mixture was centrifugated at 180 x g at 20˚C for 2 min, and the upper organic phase was transferred to a GC vial. Analysis was performed on a Shimadzu GC-2010 Plus GC-MS-TQ 8030 (Shimadzu) device with a DB-5 MS column (30 m x 0.25 mm; film thickness; 0.25 μm). GC-MS spectra were acquired as previously described (25).

Cell lines and immune cell culture. Mouse skin-derived B16F10 melanoma (Korean Cell Line Bank; Korean Cell Line Research Foundation) and the HaCaT human keratinocyte cell line (Cytion) were cultured in DMEM supplemented with 10% FBS and 1% penicillin-streptomycin (all Gibco; Thermo Fisher Scientific, Inc.). Cells were maintained at 37˚C in a 5% CO_2 atmosphere and sub-cultured every 3 days by seeding $1x10^6$ cells/T-75 flask. All experiments were conducted using cells at passages 5-8. Mycoplasma contamination testing was performed regularly to ensure cell line integrity.

Bone marrow-derived dendritic cells (BMDCs) were generated from C57BL/6 mice (Orient Bio Inc.). Female mice (n=4; age 7 weeks, weight, ~18 g) were acclimated for 1 week at the Korea Research Institute of Bioscience and Biotechnology animal facility under specific pathogen-free conditions

Table I. Antibodies used for western blotting.

Name	Supplier	Cat. no.	Dilution
Microphthalmia-associated transcription factor	Santa Cruz Biotechnology, Inc.	sc-515925	1:1,000
Tyrosinase	Santa Cruz Biotechnology, Inc.	sc-20035	1:1,000
TRP-1	Santa Cruz Biotechnology, Inc.	sc-58438	1:1,000
TRP-2	Santa Cruz Biotechnology, Inc.	sc-74439	1:1,000
p-Akt	Cell Signaling Technology, Inc.	4060S	1:1,000
p-GSK3β	Cell Signaling Technology, Inc.	5558S	1:1,000
p-ERK	Cell Signaling Technology, Inc.	4370S	1:1,000
ERK	Cell Signaling Technology, Inc.	4695S	1:1,000
p-p38	Cell Signaling Technology, Inc.	4511S	1:1,000
p38	Cell Signaling Technology, Inc.	8690S	1:1,000
p-JNK	Cell Signaling Technology, Inc.	4668S	1:1,000
JNK	Cell Signaling Technology, Inc.	9252S	1:1,000
β-actin	Santa Cruz Biotechnology, Inc.	sc-8432	1:2,000

TRP, tyrosinase related protein; p, phosphorylated; GSK3β, glycogen synthase kinase 3β.

(22±2˚C; 12/12 h light/dark cycle; 55±5% humidity), with *ad libitum* access to food and water. Mice were anesthetized with 2-3 % isoflurane (Hana Pharm Co., Ltd.) and euthanized by cervical dislocation. Bone marrow cells were isolated from femurs and tibias and cultured in RPMI-1640 medium (Gibco; Thermo Fisher Scientific, Inc.) supplemented with 10% FBS, 2.5 ng/ml IL-4 and 20 ng/ml granulocyte-macrophage colony-stimulating factor (both JW CreaGene). Cells were incubated at 37˚C with 5% CO_2 for 8 days to induce BMDC differentiation.

Cell viability. B16F10 and HaCaT cells and BMDCs ($1x10^4$ cells/well) were placed in a 96-well plate, incubated for 24 h, then treated with CSS-NPs (5-100 μg/ml) for 24 h at 37˚C in a 5% CO_2 incubator. Subsequently, the effect of CSS-NPs on cell viability was assessed using an EZ-Cytox assay kit (Dogenbio Co., Ltd.) according to the manufacturer's instructions. The EZ-Cytox solution (1X) was added to each well, and the plates were incubated at 37˚C for 30 min. Absorbance was measured at 450 nm using a SpectraMax iD5 microplate reader (Molecular Devices, LLC). To evaluate the cytotoxicity of CSS-NPs, B16F10 and HaCaT cells and BMDCs were seeded in a 12-well plate ($1x10^6$ cells/well) and treated with CSS-NPs at concentrations of 50 and 100 μg/ml, respectively, for 24 h at 37˚C. Cells were stained using an apoptosis and necrosis detection kit (Thermo Fisher Scientific, Inc.), which included Annexin V and propidium iodide, according to the manufacturer's instructions. Live and dead cells were counted using a Life Launch Attune Nxt Flow Cytometer (Thermo Fisher Scientific, Inc.) and FlowJo software (Version 10; Tree Star, Inc.).

Analysis of melanin content. B16F10 cells were seeded at a density of $1x10^5$ cells/well in a six-well plate for 24 h. Then, the cells were incubated with 5, 25, 50 and 100 μg/ml CSS-NPs at 37˚C for 3 days in the presence of α-melanocyte stimulating hormone (α-MSH; 100 nM). Cells were collected via trypsin solution (Gibco; Thermo Fisher Scientific, Inc.) and centrifuged at 8,000 x g at 20˚C for 3 min. The supernatant was removed, and cell pellets were washed twice with PBS. Cell pellets were lysed with 100 μl mixed lysis solution (1 M NaOH and 10% DMSO) and heated to 100˚C for 1 h. The solubilized melanin was transferred to a 96-well plate and the absorbance at 405 nm was measured using a SpectraMax iD5 microplate reader. The amount of solubilized melanin was normalized to the total protein content of the lysate using Pierce™ BCA Protein Assay kit.

Tyrosinase (TYR) activity. B16F10 cells ($1.5x10^5$/well in a six-well plate) were treated with 25 μg/ml CSS-NPs for 2 days at 37˚C in the presence of α-MSH (100 nM), harvested and washed twice in PBS. TYR activity was measured using the TYR assay kit (cat. no. MAK550-1KT; MilliporeSigma) according to the manufacturer's instructions.

Western blotting. B16F10 cells ($0.5x10^5$/per well in a six-well plate) were incubated with 5 or 25 μg/ml CSS-NPs for 2 days at 37˚C in the presence of α-MSH (100 nM). Cells were lysed in M-PER Mammalian Protein Extraction Reagent and Halt Protease & Phosphatase Inhibitor Cocktail (Thermo Fisher Scientific, Inc.) according to the manufacturer's instructions. The protein was quantified using the BCA kit, and protein samples were denatured for 10 min at 70˚C. Subsequently, 25 μg/lane protein was separated using 4-12% SDS-PAGE, transferred onto PVDF membranes (Thermo Fisher Scientific, Inc.) and blocked with EveryBlot Blocking Buffer (cat. no. #12010020; Bio-Rad Laboratories, Inc.) at 25˚C for 1 h. The membrane was then incubated with primary antibodies at 4˚C for 24 h (Table I). The membrane was incubated with anti-mouse (1:10,000; cat. no. 7076S) or rabbit IgG (1:10,000; Cat. no. 7074S; both Cell signaling technology, Inc.) HRP-linked secondary antibodies at 25˚C for 1 h. Protein bands were detected using enhanced SuperSignal West Pico PLUS

Table II. Primers used for reverse transcription-quantitative PCR.

Gene	Sequence, 5'→3'
Microphthalmia-associated transcription factor	CCCGTCTCTGGAAACTTGATCG (forward)
	CTGTACTCTGAGCAGCAGGTG (reverse)
Tyrosinase	GTCGTCACCCTGAAAATCCTAACT (forward)
	CATCGCATAAAACCTGATGGC (reverse)
TRP-1	GCTGCAGGAGCCTTCTTTCT (forward)
	AAGACGCTGCACTGCTGGTC (reverse)
TRP-2	TTGCCCTACTGGAACTTTGC (forward)
	TGGGTCATCTTGTCTTGCTG (reverse)
β-actin	TATTGGCAACGAGCGGTTCC (forward)
	GGCATAGAGGTCTTTACGGATGTC (reverse)

TRP, tyrosinase-related protein.

chemiluminescence substrates (Thermo Fisher Scientific, Inc.) and visualized using Amersham ImageQuant™ 800 (Cytiva, Amersham, England). Densitometry was quantified using the ImageQuant TL analysis software (Cytiva, version 10.0.261).

mRNA analysis. B16F10 cells (1x10^5/well in a 12-well plate) were incubated with CSS-NPs (5 and 25 μg/ml) and α-MSH (100 nM) for 24 h at 37˚C. Cells were washed twice in PBS, and total RNA was isolated using a RNeasy Mini kit (Cat no. 74106; Qiagen GmbH). For reverse transcription-quantitative (RT-q) PCR, 10 μl RNA was reverse-transcribed into cDNA using the iScript Adv cDNA kit for RT-qPCR (Cat. no. #1725038; Bio-Rad Laboratories, Inc.), according to the manufacturer's instructions. Next, target cDNA levels were quantified by RT-qPCR using the CFX96 Touch RT-PCR detection system and SYBR green (Bio-Rad Laboratories, Inc.). The PCR steps for all genes were as follows: For a hot start, 40 cycles of 95˚C for 5 min, 95˚C for 20 sec, 60˚C for 20 sec and 72˚C for 30 s, melting curve at 95˚C for 1 min, 55˚C for 1 min, and 30˚C for 1 min. The quantification of gene expression was performed using the 2^-ΔΔCq method (26). Specific forward and reverse primers are presented in Table II.

Inhibitor assay. B16F10 cells were seeded (0.5x10^5/per well in a six-well plate) and pretreated with PD98059 (ERK inhibitor, 20 μM) or LY294002 (PI3K inhibitor, 10 μM) at 37˚C for 1 h before treatment with 25 μg/ml CSS-NPs and α-MSH (100 nM) at 37˚C. After 2 days, cells were harvested for subsequent experiments.

2,2-diphenyl-1-picrylhydrazyl (DPPH) assay. DPPH radical scavenging activity of CSS-NPs was determined as previously described (27). The samples, diluted to specific concentrations (0.1, 0.2, 0.5 and 1 mg/ml) with distilled water, were mixed with 0.2 mM DPPH solution (MilliporeSigma) at a 1:1 ratio (100 μl each). The mixture was stirred and left to stand in the dark for 30 min at 20˚C, after which the absorbance was measured at 517 nm using a SpectraMax iD5 microplate reader.

2,2'-Azino-bis (3-ethylbenzothiazoline-6-sulfonic acid) diammonium salt (ABTS) assay. ABTS radical scavenging activity of CSS-NPs was determined as previously described (28). To prepare the ABTS solution, 88 μl 140 mM potassium persulfate (Samchun Pure Chemical Co., Ltd.) and two ABTS diammonium salt tablets (MilliporeSigma) were added to 5 ml distilled water, mixed thoroughly, and allowed to react in the dark for 12-16 h at 20˚C. ABTS solution was diluted with 95% ethanol at a ratio of 1:88 to achieve an absorbance of 0.7±0.02 at 734 nm. A total of 50 μl sample, diluted to specific concentrations (0.1, 0.2, 0.5 and 1.0 mg/ml) with distilled water, was mixed with 1 ml ABTS solution. Finally, the mixture was stirred and allowed to react in the dark for 5 min at 20˚C, and the absorbance was measured at 734 nm.

Measurement of ROS. B16F10 cells (1/10^5/well) were seeded in 12-well plates and incubated with CSS-NPs and vitamin C (Vit C; both 50 μg/ml) in the presence of α-MSH (100 nM) for 24 h at 37˚C. Following cell harvesting, intracellular ROS levels were measured using a CellROX kit (Thermo Fisher Scientific, Inc.), according to the manufacturer's protocol.

Antioxidant activity. Total antioxidant capacity (TAC) and catalase (CAT) enzyme activity in sonicated (40 kHz at 25˚C for 5 min) lysate of B16F10 cells treated with CSS-NPs and Vit C (both 50 μg/ml) for 24 h at 37˚C in the presence of α-MSH (100 nM) were measured using EZ-Total Antioxidant Capacity (Dogenbio Co., Ltd.) and Catalase Colorimetric Assay (Thermo Fisher Scientific, Inc.). kits, respectively, according to the manufacturers' protocols.

Statistical analysis. All data are expressed as the mean ± standard deviation of three independent experiments. Significance of groups was evaluated using one-way ANOVA followed by Tukey's multiple comparison test. Data were analyzed using GraphPad Prism 9 (Dotmatics), $P<0.05$ was considered to indicate a statistically significant difference.

Results

Profiling and stability of CSS-NPs. CSS-NPs were isolated from CSS using TFF and sucrose cushioned ultracentrifugation, resulting in highly purified nanoparticles (Fig. 1A). The

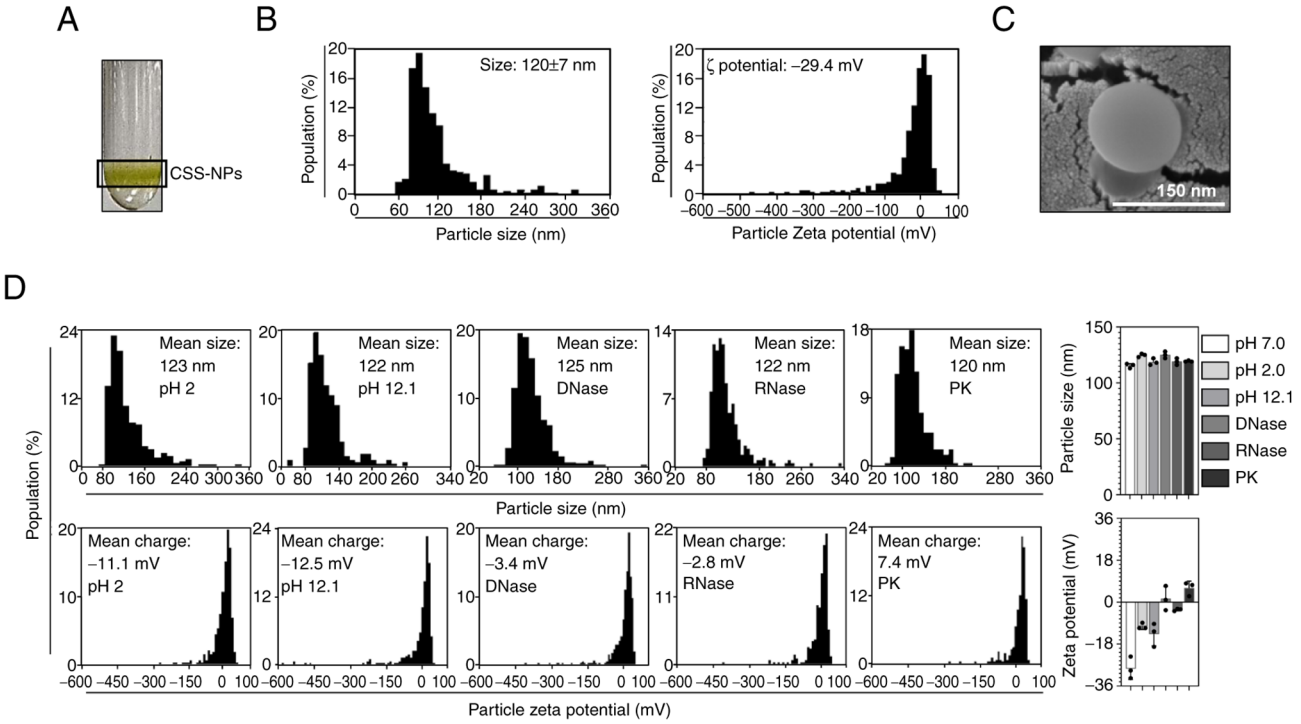

Figure 1. Characterization and stability of CSS-NPs under external stress. (A) Purified CSS-NPs obtained by concentrating CSS juice using a tangential flow filtration system, followed by cushioned ultracentrifugation. (B) Size distribution and ζ potential of CSS-NPs resuspended in phosphate-buffered saline at a pH of 7.0 analyzed using qNano-Exoid. (C) Structural analysis of CSS-NPs by scanning electron microscopy. (D) Stability of CSS-NPs following exposure to acidic (pH 2.0) and alkaline (pH 12.1) environments and enzymes. CSS-NP, *Cannabis sativa* stem-derived nanoparticle; PK.

purified CSS-NPs were characterized by size, ζ potential and morphological features using qNano-Exoid (Fig. 1B) and SEM (Fig. 1C). CSS-NPs, when resuspended in PBS at a pH of 7.0, had a mean diameter of 120±7 nm. The ζ potential value was -29.4 mV (Fig. 1B), which falls within the stable range (-30-30 mV) for nanoparticles (29). SEM imaging confirmed that CSS-NPs possessed typical nanovesicle structure characterized by spherical morphology (Fig. 1C). Notably, CSS-NPs maintained consistent particle size and ζ potential values within the stable range across acidic (pH 2.0) and alkaline (pH 12.1) conditions, compared with those in the neutral condition (pH 7.0), and following exposure to DNase, RNase and proteinase K (Fig 1D). This demonstrated that CSS-NPs exhibit stability under external stress conditions.

Biochemical composition analysis of CSS-NPs. Next, the biochemical composition of CSS-NPs was analyzed using UPLC/Q-TOF-MS (Fig. 2A and Table III) and GC-MS (Fig. 2B and Table IV). A total of 48 metabolites were detected within the CSS-NPs. UPLC/Q-TOF-MS analysis identified four nucleosides, three amino acids, two flavonoids and 20 lipids and chlorophyll derivatives (Fig. 2A; Table II). The nucleosides were guanine, adenosine, guanosine and 1-methyladenosine; the amino acids were N-(1-deoxy-1-fructosyl) valine, L-phenylalanine and L-tryptophan and the flavonoids were pterosin E and pterosin K. Furthermore, CSS-NPs contained pheophorbide A, a chlorophyll derivative. CSS-NPs contained various lipid compositions including dehydrophytosphingosine, 3-ketosphingosine, phytosphingosine, stearoylethanolamide, lysophosphatidylcholine 16:0 (lysoPC 16:0), 2-O-protocatechuoylalphitolic acid, PC[18:1(9Z)/2:0], methyl 4,8-decadienoate, lysoPC(18:0), lysoPC[16:1(9Z)], PC[16:1(9Z)/17:1(9Z)], lysoPC[18:1(9Z)], PC[17:1(9Z)/17:1(9Z)], lysoPC[22:6(4Z,7Z,10Z,13Z,16Z,19Z)], PC(18:0/2:0), 13-docosenamide, octadecanamide, oleoylethanolamide, stigmastane-3,6-dione and PC[18:3(9Z,12Z,15Z)/16:0]. In GC-MS analysis, an additional 18 metabolites were identified, including glycerol, ribose, threose, xylose, lyxose, arabinose, rhamnose, fructofuranose, psicofuranose, tagatose, pinitol, fructose, talose, glucose, galactose, palmitic acid, myo-inositol and stearic acid (Fig. 2B and Table IV).

Cytotoxic effects of CSS-NPs in different cell types. Cytotoxic effects of CSS-NPs were observed in B16F10 and HaCaT cells and BMDCs. CSS-NPs treatment did not affect cellular cytotoxicity, and B16F10 cell viability remained unchanged at concentrations of 5-50 μg/ml but revealed a significant increase at a concentration of 100 μg/ml. By contrast, HaCaT cells and BMDCs exhibited no significant changes in viability up to 100 μg/ml (Fig. 3A). Annexin V and PI staining confirmed that no death occurred in any of the cells treated with CSS-NPs at 50 or 100 μg/ml (Fig. 3B). These findings demonstrate that CSS-NPs did not exhibit cytotoxicity and that the selected concentrations were appropriate for assessing the whitening and antioxidant activity of CSS-NPs in melanoma cells.

CSS-NPs suppress melanin synthesis in α-MSH-stimulated B16F10 cells. CSS-NPs inhibited melanin formation in a dose-dependent manner (Fig. 3C). Melanin synthesis is catalyzed by three enzymes: TYR and tyrosinase-related protein (TRP)-1 and TRP-2, with TYR being an enzyme

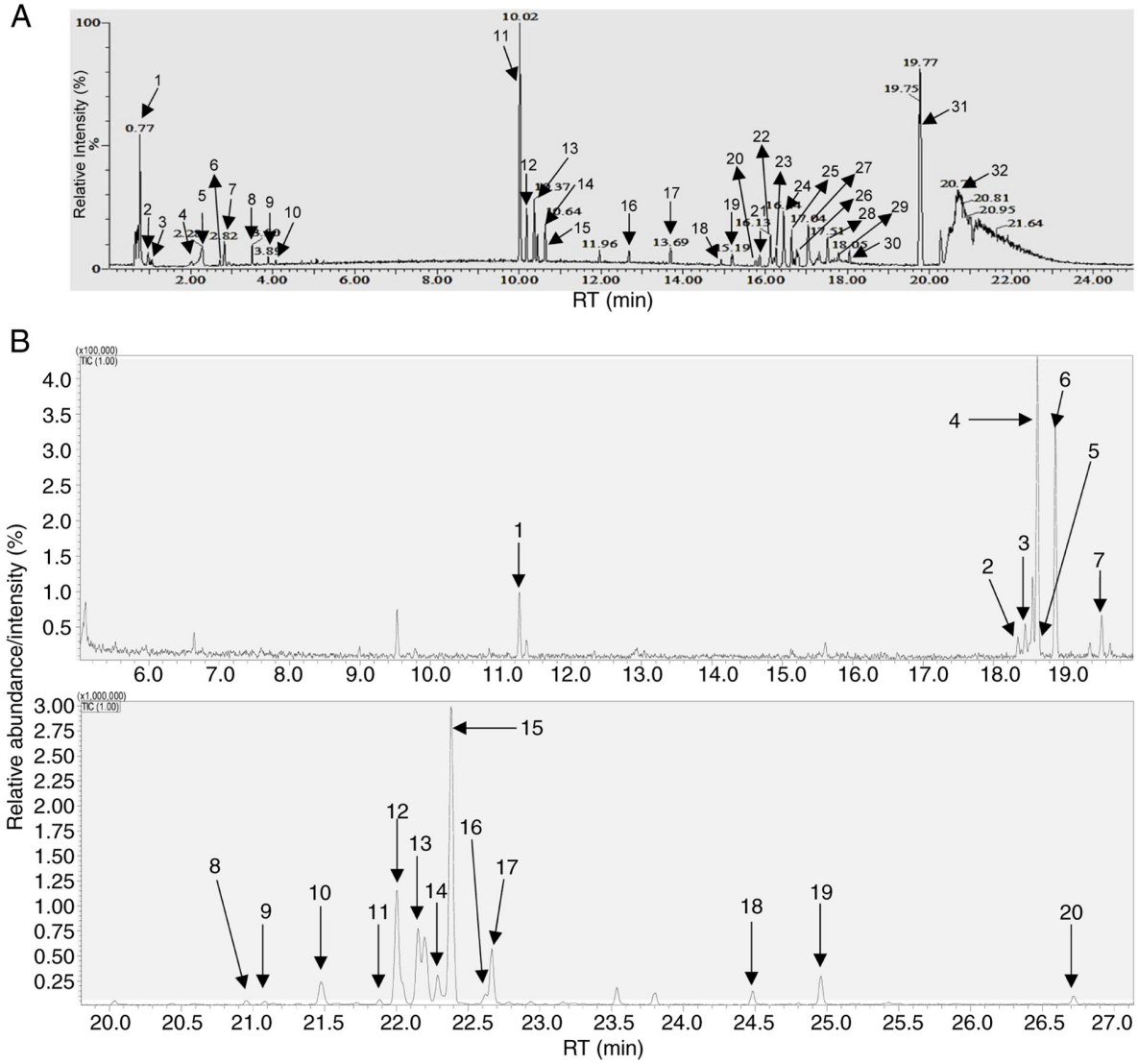

Figure 2. Metabolite composition of CSS-NPs. Metabolite analysis of CSS-NPs using (A) ultra-performance liquid chromatography/quadrupole-time-of-flight mass spectrometry and (B) gas chromatography-mass spectrometry. CSS-NP, *Cannabis sativa* stem-derived nanoparticle; TIC, total ion chromatogram.

that initiates melanin synthesis (30,31). Therefore, TYR activity was measured in B16F10 cells treated with CSS-NPs. Compared with the control (α-MSH-treated B16F10 cells), low-dose CSS-NPs (25 μg/ml) resulted in decrease TYR activity (Fig. 3D), suggesting that CSS-NPs regulate melanin synthesis by modulating TYR activity.

CSS-NPs downregulate the melanogenic signaling pathway and gene expression in α-MSH-stimulated B16F10 cells. Microphthalmia-associated transcription factor (MITF) is a key transcription factor that controls the activity levels of TYR, TRP-1 and TRP-2 in melanogenesis (32). Thus, to explore how CSS-NPs affect the regulatory mechanisms of melanin synthesis induced by α-MSH in B16F10 cells, western blot analysis was performed out. Protein expression levels of MITF, TYR, TRP-1 and TRP-2 decreased in cells treated with 5 and 25 μg/ml CSS-NPs compared with those treated with α-MSH alone (Fig. 4A). CSS-NPs significantly inhibited the expression of melanin synthesis-associated genes including MITF, TYR, TRP-1 and TRP-2 (Fig. 4B). These results suggested that the anti-melanogenic effects of CSS-NPs in B16F10 cells were induced by downregulation of melanogenic genes and protein including MITF, TYR, TRP-1 and TRP-2.

CSS-NPs activate ERK and Akt signaling in α-MSH-stimulated B16F10 cells. MAPK signaling regulates cellular processes by transducing external signals into intracellular responses (33). Therefore, whether MAPK signaling regulated the anti-melanogenic activity induced by CSS-NPs was evaluated. CSS-NPs dose-dependently increased the phosphorylation of ERK, but not JNK and p38 (Fig. 5A). To elucidate the functional role of CSS-NPs in activating ERK signaling in α-MSH-stimulated B16F10 cells, melanin content and biosynthesis proteins in the presence of PD98059 (an ERK inhibitor) were assessed. Melanin content (Fig 5B) and biosynthesis protein levels (MITF, TYR, TRP-1 and TRP-2; Fig. 5C), which were decreased by CSS-NPs in α-MSH-treated B16F10 cells, increased when ERK signaling (PD98059-treated condition) was inhibited. Subsequently, the PI3K/Akt signaling pathway was investigated because this signaling pathway

Table III. Ultra-high-performance liquid chromatography quadrupole time-of-flight mass spectrometry analysis of *Cannabis sativa* stem-derived nanoparticles.

No.	Retention time (min)	Identification	Mass-to-charge ratio	Fragment ions (m/z)
1	0.77	Guanine	152.05	136
2	0.96			136,119
3	1.05	N-(1-Deoxy-1-fructosyl)valine	280.14	262, 244, 118, 112, 91, 87, 84
4	2.03	Adenosine	268.10	136, 119
5	2.28	Guanosine	284.10	152, 135, 110
6	2.68	1-Methyladenosine	282.12	136, 119
7	2.82	L-phenylalanine	166.08	120, 103, 91, 77
8	3.50	L-tryptophan	205.0	188, 146, 118, 115, 91
9	3.89	Pterosin E	233.05	215, 203, 177, 169, 147, 79
10	4.08	Pterosin K	267.13	237, 217
11	10.02	Dehydrophytosphingosine	316.28	298, 280, 209, 125
12	10.18	3-Ketosphingosine	298.27	280, 109, 95, 81, 69
13	10.37			280, 193, 95, 83, 81, 69
14	10.45	Phytosphingosine	318.30	300, 69
15	10.64	Stearoylethanolamide	328.29	251, 83
16	12.68	LysoPC(16:0)	496.33	184, 104
17	13.69	2-O-Protocatechuoylalphitolic acid	609.34	177
18	14.91	PC(18:1(9Z)/2:0)	564.42	184
19	15.19	Methyl 4,8-decadienoate	183.08	165, 153, 109, 107, 95, 81
20	15.77	Pheophorbide A	593.28	577, 533, 519, 475, 447, 433
21	15.85	LysoPC(18:0)	524.51	313, 184
22	16.13	LysoPC(16:1(9Z))	494.56	337, 313, 184
23	16.26	PC16:1(9Z)/17:1(9Z))	744.64	337, 184
24	16.44	LysoPC(18:1(9Z))	522.60	337, 184
25	16.65	PC(17:1(9Z)/17:1(9Z))	758.56	337, 184
26	16.78	LysoPC(22:6(4Z, 7Z, 10Z, 13Z, 16Z, 19Z))	568.43	184
27	17.04	PC(18:0/2:0)	566.55	184
28	17.51	13-Docosenamide	338.34	184, 121, 109, 95, 81
29	17.80	Octadecanamide	284.29	243, 211, 201, 95
30	18.05	Oleoylethanolamide	326.34	237, 209, 109, 95
31	19.77	Stigmastane-3,6-dione	429.37	177, 139, 121, 107, 95, 81
32	20.70	PC(18:3(9Z, 12Z, 15Z)/16:0)	756.55	337, 313, 184

regulates melanin synthesis by promoting the degradation of MITF (34). CSS-NPs promoted an increase of Akt phosphorylation and consequent decrease of GSK3β phosphorylation in α-MSH-treated B16F10 cells (Fig. 6A). Following inhibition of Akt signaling (LY294002-treated condition), CSS-NPs restored the melanin content (Fig. 6B). Additionally, expression of melanin biosynthesis proteins increased following α-MSH treatment (Fig. 6C). These results indicate that CSS-NPs suppressed melanin synthesis by activating the ERK and Akt signaling pathway.

CSS-NPs restore antioxidant activity in α-MSH-stimulated B16F10 cells. Synthesis of melanin leads to an increase in ROS within skin cells, which is associated with skin aging, pigmentation alteration and the onset of inflammatory reactions (35-37). To determine whether CSS-NPs exert antioxidant effects by controlling ROS generated during melanin synthesis, the indirect antioxidant potential of CSS-NPs was assessed using DPPH and ABTS radical scavenging assays, with Vit C serving as a positive control. CSS-NPs exhibited lower direct radical scavenging activity than Vit C; however, the activity of CSS-NPs increased in a concentration-dependent manner; these results were not significant (Fig. 7A). Whether CSS-NPs could provide protection in α-MSH-stimulated B16F10 cells at non-toxic concentrations was evaluated. CSS-NPs restored cell viability in a dose-dependent manner (Fig. 7B). The antioxidant functionality of CSS-NPs was explored by comparing their effects on cellular toxicity induced during melanin synthesis with those of Vit C. CSS-NPs effectively reduced α-MSH-induced cytotoxicity, demonstrating effects comparable with treatment with Vit C (Fig. 7C). Finally, to investigate the underlying mechanism, intracellular ROS

Table IV. Gas chromatography mass spectrometry analysis of *Cannabis sativa* stem-derived nanoparticles.

No.	Compound	Retention time, min)	Retention index	Area
1	Glycerol	11.265	1269	173000
2	Ribose	18.349	1640	54664
3	Threose	18.45	1646	108640
4	Xylose	18.554	1652	239424
5	Lyxose	18.624	1656	934454
6	Arabinose	18.879	1671	687705
7	Rhamnose	19.539	1709	110111
8	Fructofuranose	20.954	1795	97657
9	Psicofuranose	21.082	1803	73027
10	Tagatose	21.475	1829	580484
11	Pinitol	21.883	1855	87359
12	Fructose	22.003	1863	2721573
13		22.151	1872	1688900
14	Talose	22.287	1881	677544
15	Glucose	22.382	1887	5921962
16		22.621	1903	198221
17	Galactose	22.665	1906	1046570
18	Palmitic acid	24.482	2043	241181
19	myo-inositol	24.958	2082	533891
20	Stearic acid	26.717	2239	165370

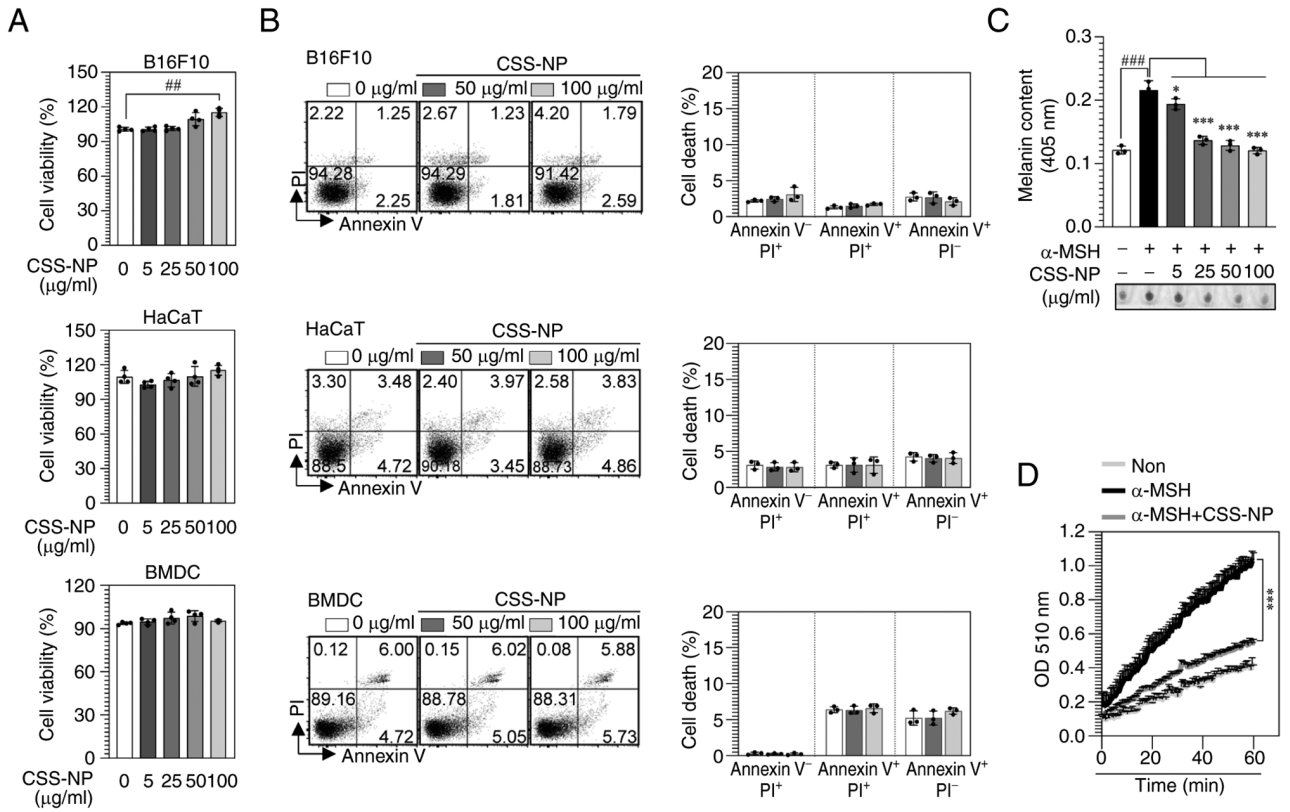

Figure 3. Cellular toxicity and anti-melanogenic activity of CSS-NPs. (A) Viability of melanoma cells (B16F10), keratinocytes (HaCaT) and BMDCs treated with CSS-NPs assessed using the EZ-Cytox assay kit. (B) Cytotoxic effects on B16F10 and HaCaT cells and BMDCs treated with CSS-NPs evaluated using Annexin V and PI staining. Annexin V^-PI^+ cells indicate necrosis; Annexin V^+PI^+ cells indicate late apoptosis; Annexin V^+PI^- cells indicate early apoptosis. (C) Melanin levels in α-MSH-induced B16F10 cells following treatment with CSS-NPs for 72 h. (D) Tyrosinase activity in α-MSH-induced B16F10 cells treated with CSS-NPs (25 μg/ml) measured using a tyrosinase inhibitor screening kit. *P<0.05, ***P<0.001 vs. α-MSH-treated; $^{\#\#}$P<0.01, $^{\#\#\#}$P<0.001 vs. non-treated cells. CSS-NP, *Cannabis sativa* stem-derived nanoparticle; BMDC, bone marrow-derived dendritic cell; PI, propidium iodide; α-MSH, α-melanocyte stimulating hormone; OD, optical density.

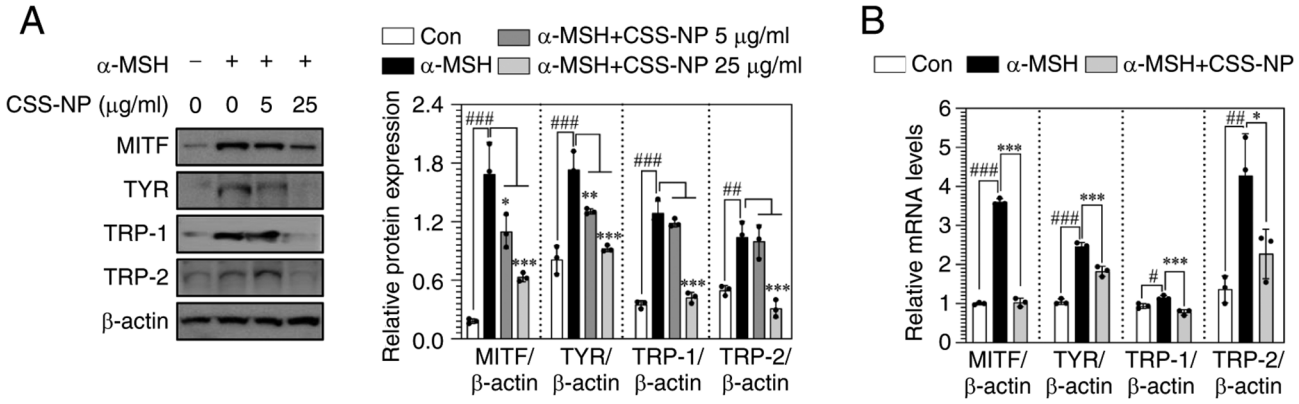

Figure 4. Melanin synthesis-associated mRNA and protein levels induced by CSS-NPs in α-MSH-treated B16F10 cells. B16F10 cells were treated with CSS-NPs (5 and 25 μg/ml) in the presence of α-MSH (100 nM). (A) Protein expression of MITF, TYR, TRP-1 and TRP-2 determined by western blotting. β-actin was used as a protein loading control. (B) mRNA levels of MITF, TYR, TRP-1 and TRP-2 determined by reverse transcription-quantitative PCR. *P<0.05, **P<0.01, ***P<0.001 vs. α-MSH-treated cells and $^{\#}$P<0.05, $^{\#\#}$P<0.01, $^{\#\#\#}$P<0.001 vs. non-treated cells. CSS-NP, *Cannabis sativa* stem-derived nanoparticle; MITF, microphthalmia-associated transcription factor; TYR, tyrosinase; TRP, tyrosinase-related protein; α-melanocyte stimulating hormone, α-MSH; Con, control.

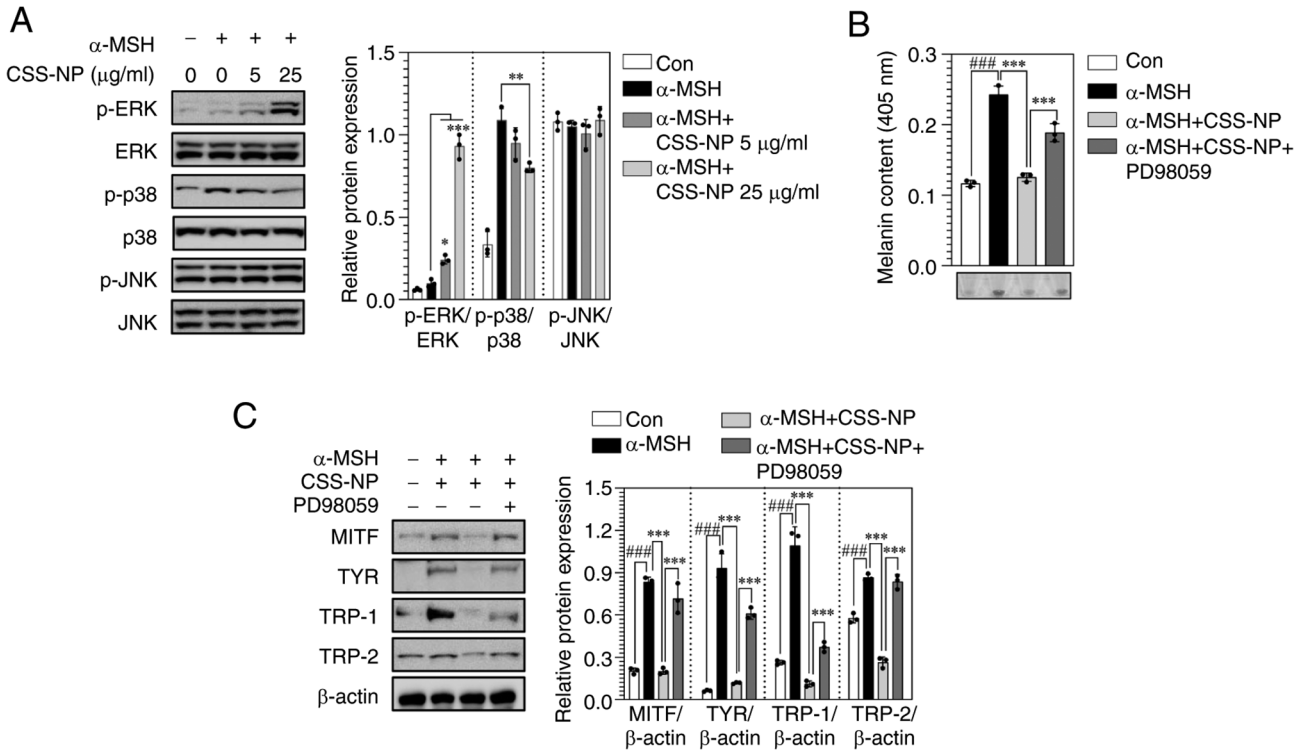

Figure 5. Changes in MAPK signaling pathway induced by CSS-NPs in α-MSH-treated B16F10 cells. (A) Western blot analysis of protein expression of MAPKs (ERK, p38, and JNK) in B16F10 cells treated with CSS-NPs at 5 and 25 μg/ml for 2 days in the presence of 100 nM α-MSH. (B) Melanin content and (C) western blot analysis of expression of MITF, TYR, TRP-1 and TRP-2 in α-MSH-treated B16F10 cells co-treated with PD98059 (ERK inhibitor; 10 μM) and CSS-NPs (25 μg/ml) for 3 days. *P<0.05, **P<0.01, ***P<0.001 vs. α-MSH-treated or α-MSH + CSS-NPs; $^{\#\#\#}$P<0.001 vs. non-treated cells. CSS-NP, *Cannabis sativa* stem-derived nanoparticle; α-MSH, α-melanocyte stimulating hormone; MITF, microphthalmia-associated transcription factor; TYR, tyrosinase; TRP, tyrosinase-related protein; Con, control; p-, phosphorylated.

levels (Fig. 7D) and antioxidant enzyme activity (TAC and CAT; Fig. 7E) were measured. In α-MSH-stimulated B16F10 cells treated with CSS-NPs, intracellular ROS levels were significantly decreased, while TAC and CAT activities were increased compared with α-MSH-stimulated B16F10 cells. These effects were similar to those observed with Vit C treatment. These results suggest that CSS-NPs preserved melanocyte survival by suppressing free radicals generated during excessive melanin formation and alleviating impaired antioxidant activity.

Discussion

The present study suggested that CSS-NPs are a reliable natural material with potential as a cosmetic ingredient. CSS-NPs contained 48 primary bioactive metabolites

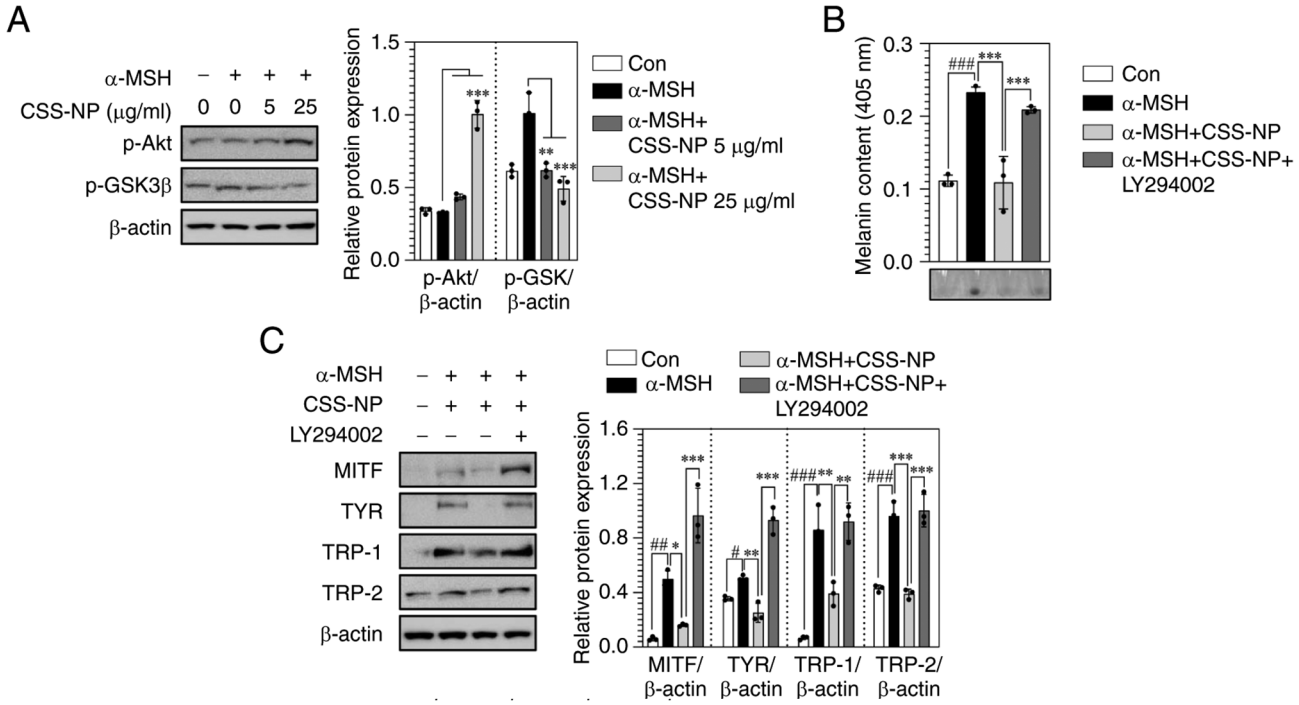

Figure 6. Change in the Akt signaling pathway induced by CSS-NPs in α-MSH-treated B16F10 cells. (A) Protein expression of p-Akt and p-GSK3β determined by western blotting in B16F10 cells treated with CSS-NPs at 5 and 25 μg/ml for 2 days in the presence of 100 nM α-MSH. (B) Melanin content and (C) protein expression of MITF, TYR, TRP-1 and TRP-2 determined using western blotting in α-MSH-treated B16F10 cells co-treated with LY294002 (Akt inhibitor; 20 μM) and CSS-NPs (25 μg/ml) for 3 days. β-actin was used as a protein loading control. *P<0.05, **P<0.01, ***P<0.001 vs. α-MSH-treated or α-MSH + CSS-NPs; $^{\#}$P<0.05, $^{\#\#}$P<0.01, $^{\#\#\#}$P<0.001 vs. non-treated cells. CSS-NP, *Cannabis sativa* stem-derived nanoparticle; GSK3β, glycogen synthase kinase 3β; α-MSH, α-melanocyte stimulating hormone; MITF, microphthalmia-associated transcription factor; TYR, tyrosinase; TRP, tyrosinase-related protein; Con, control; p-, phosphorylated.

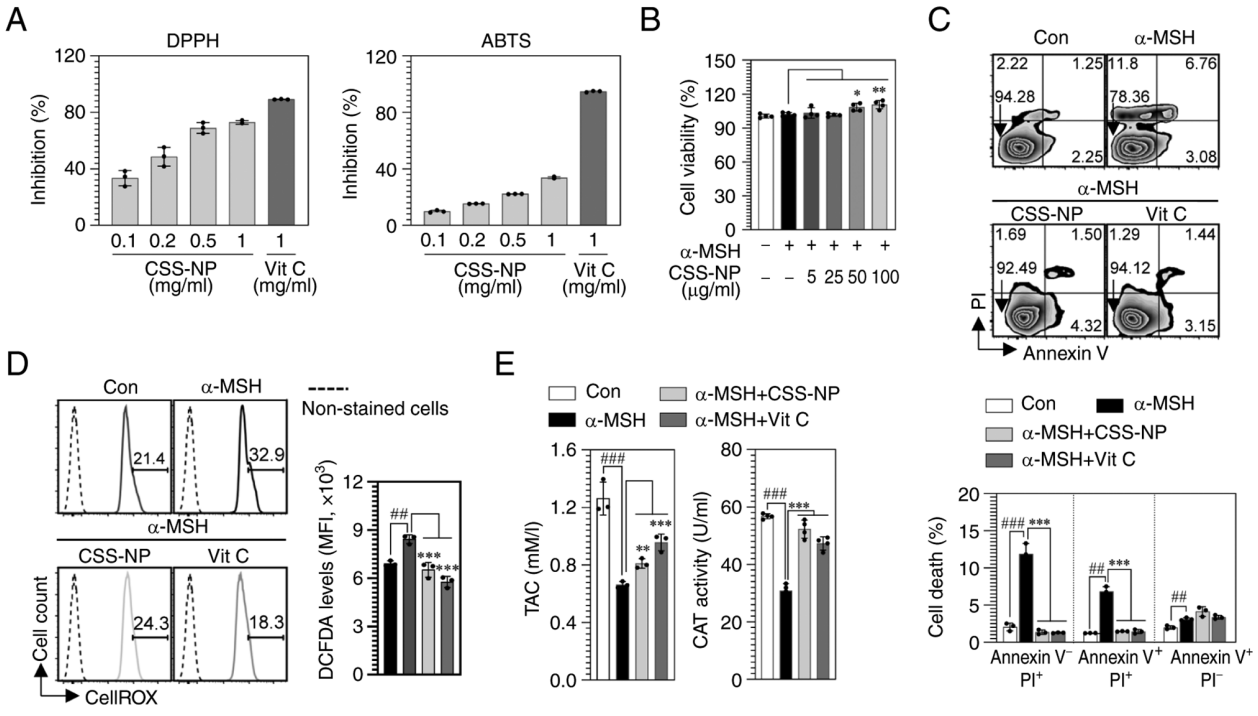

Figure 7. Antioxidant activity induced by CSS-NPs in α-MSH-treated B16F10 cells. (A) Radical scavenging activity assessed by DPPH and ABTS. (B) Viability of B16F10 cells co-treated with 5, 25, 50 and 100 μg/ml CSS-NPs for 2 days in the presence of 100 nM α-MSH, measured using an EZ-Cytox assay kit. (C) Cytotoxic effects in α-MSH-treated B16F10 cells co-stimulated with CSS-NPs or Vit C (both 50 μg/ml) were evaluated using Annexin V and propidium iodide staining. (D) Reactive oxygen species levels in α-MSH-treated B16F10 cells co-stimulated with CSS-NPs or Vit C analyzed using a CellROX kit. (E) TAC and CAT activity in α-MSH-treated B16F10 cells co-stimulated with CSS-NPs or Vit C (50 μg/ml) detected using TAC and CAT detection kits. *P<0.05, **P<0.01, ***P<0.001 vs. α-MSH-treated ; $^{\#\#}$P<0.01, $^{\#\#\#}$P<0.001 vs. non-treated cells. CSS-NP, *Cannabis sativa* stem-derived nanoparticle; α-MSH, α-melanocyte stimulating hormone, Vit C, vitamin C; Con, control; TAC, total antioxidant capacity; CAT, catalase; DDPH, 2,2-diphenyl-1-picrylhydrazyl; ABTS, 2,2'-azino-bis(3-ethylbenzothiazoline-6-sulfonic acid) diammonium.

and exhibited significant resistance to pH fluctuations and enzymatic reactions, such as DNase, RNase and proteinase K. CSS-NPs decreased the expression of key factors involved in melanin synthesis by activating the ERK and Akt signaling pathways under excessive melanin production in B16F10 cells. Additionally, the present study demonstrated that CSS-NPs alleviated melanocyte toxicity induced during excessive melanin synthesis, which may be attributed to the suppression of ROS and the upregulation of antioxidant enzymes.

CSS-NPs exerted an anti-melanogenic effect by down-regulating TYR activity, as well as TRP-1, TRP-2 and MITF gene and protein expressions. TYR, TRP-1 and TRP-2 are key enzymes in melanin biosynthesis. MITF, the key activator of these genes or proteins, is a central transcription factor that regulates melanin synthesis and governs the proliferation, differentiation and survival of melanocytes (38,39). Materials capable of controlling these melanin synthesis factors can offer considerable advantages in developing effective skin-whitening products, such as enhancing skin brightening efficacy, reducing hyperpigmentation, and providing a safer alternative to conventional depigmenting agents like hydroquinone.

The anti-melanogenic effect induced by CSS-NPs may be associated with the activation of the ERK and Akt signaling pathways. The ERK and Akt signaling pathways are associated with the transcriptional activation and stabilization of MITF (40,41). Accordingly, research aims to identify candidate substances that regulate the ERK and Akt signaling pathways; however, this faces challenges owing to the potential for side effects (42-45). Examples of such candidate substances include gomisin N and berberine, which is a component of various plant species (42,43). These compounds inhibit melanin production through ERK and Akt pathway activation; however, clinical research is still in its early phases, and cytotoxicity has been observed at high concentrations (44,45). The present study revealed that CSS-NPs significantly inhibited melanin production without exhibiting toxicity. Additionally, mechanistic experiments using ERK- and Akt-specific pharmacological inhibitors revealed that the decrease in key elements associated with melanin synthesis induced by CSS-NPs could be reversed by activating the ERK and Akt pathways. Thus, CSS-NPs, with non-cytotoxic properties, may serve as novel natural cosmetic ingredients with the potential to treat skin pigmentation disorder and serve as an alternative to chemical-based cosmetics.

CSS-NPs are a multifunctional natural material, possessing not only anti-melanogenic effects but also antioxidant properties. Melanin is involved in ROS production, which causes melanocytes undergoing melanin synthesis to maintain higher ROS levels than other cell types (35). Elevated levels of ROS damage the DNA, proteins and lipids within skin cells, leading to impaired cellular function. This oxidative stress contributes to skin aging, pigmentary alteration and inflammatory responses (35,46,47). CSS-NPs could scavenge free radicals, and in conditions of excessive melanin synthesis, CSS-NPs restored antioxidant capacity within the cellular antioxidant defense system. These findings suggested that CSS-NPs can be employed as a cosmetic ingredient with multifunctional effects, capable of not only alleviating skin pigmentation disorder caused by excessive melanin synthesis but also protecting skin cells.

Plants can produce various phytochemicals beneficial to human health, which can be encapsulated within plant-derived exosomes to exert bioactive functions (48-50). GC-MS and LC-MS data provided insights into the chemical composition and potential bioactive functions of CSS-NPs. The metabolic product analysis of CSS-NPs identified 10 phospholipids, which may be involved in the nanostructure formation of CSS-NPs. CSS-NPs incorporate three compounds known for their anti-melanogenic activity (adenosine, phytosphingosine and oleoylethanolamide) and four compounds recognized for their antioxidant effects (2-O-protocatechuoylalphitolic acid, pheophorbide A, myo-inositol and stigmastane-3,6-dione). Consequently, the decreased melanin intracellular melanin synthesis by CSS-NPs and the enhancement of antioxidant effects may be due to metabolites in CSS-NPs that induce anti-melanogenic and antioxidant properties.

Despite the present study demonstrating the functional potential of CSS-NPs as a cosmetic ingredient at the cellular level, additional studies are needed to establish their practical value and reliability. To enhance the credibility and applicability of CSS-NPs, it is essential to obtain safety data through clinical studies addressing potential side effects and toxicity in humans. Once safety is confirmed, evaluation of the clinical value of CSS-NPs for various skin conditions (such as, wrinkles, hyperpigmentation, dry skin, telangiectasia and skin damage) is key for enhancing their practical value. Toxicological and clinical data may determine the value and function of CSS-NPs as a cosmetic ingredient.

The present study confirmed that CSS-NPs, which contain metabolites with anti-melanogenic and antioxidant properties, inhibited excessive melanin synthesis by inducing ERK and Akt activation. Moreover, CSS-NPs induced antioxidant effects in melanocytes by decreasing ROS levels and restoring antioxidant activity during the melanin synthesis process. These findings indicated that CSS-NPs may be used as a multifunctional ingredient in the treatment of hyperpigmentation disorder as they suppress excessive melanin production in skin cells and offer protective effects against cellular toxicity.

Acknowledgements

Not applicable.

Funding

The present study was supported by the Korea Research Institute of Bioscience and Biotechnology Research Initiative Programs (grant nos. KGM5242423 and KGM5382414).

Availability of data and materials

The data generated in the present study may be requested from the corresponding author.

Authors' contributions

HJL performed experiments, analyzed data and wrote the manuscript. YHK performed experiments and analyzed data. SJL and JCJ analyzed data. SHP designed and performed experiments. JMY performed experiments and facilitated data

interpretation. JCJ, WSK and YBR designed experiments. WSK conceived and supervised the study, performed experiments and wrote and reviewed the manuscript. YBR and WSK confirm the authenticity of all the raw data. All authors have read and approved the final manuscript.

Ethics approval and consent to participate

The present study was approved by the Institutional Animal Care and Use Committee of the Korea Research Institute of Bioscience and Biotechnology (approval no. KRIBB-AEC-24094).

Patient consent for publication

Not applicable.

Competing interests

The authors declare that they have no competing interests.

References

1. D'Mello SA, Finlay GJ, Baguley BC and Askarian-Amiri ME: Signaling pathways in melanogenesis. Int J Mol Sci 17: 1144, 2016.
2. Solano F: Photoprotection and skin pigmentation: Melanin-Related molecules and some other new agents obtained from natural sources. Molecules 25: 1537, 2020.
3. Lee A, Kim JY, Heo J, Cho DH, Kim HS, An IS, An S and Bae S: The inhibition of melanogenesis via the PKA and ERK signaling pathways by chlamydomonas reinhardtii extract in B16F10 melanoma cells and artificial human skin equivalents. J Microbiol Biotechnol 28: 2121-2132, 2018.
4. Sarkar R, Arora P and Garg KV: Cosmeceuticals for hyperpigmentation: What is available? J Cutan Aesthet Surg 6: 4-11, 2013.
5. Pillaiyar T, Manickam M and Namasivayam V: Skin whitening agents: Medicinal chemistry perspective of tyrosinase inhibitors. J Enzyme Inhib Med Chem 32: 403-425, 2017.
6. Solano F, Briganti S, Picardo M and Ghanem G: Hypopigmenting agents: An updated review on biological, chemical and clinical aspects. Pigment Cell Res 19: 550-571, 2006.
7. Kooyers T and Westerhof W: Toxicology and health risks of hydroquinone in skin lightening formulations. J European academy of Dermatology and Venereology 20: 777-780, 2006.
8. Sarasati A, Syahruddin MH, Nuryanti A, Ana ID, Barlian A, Wijaya CH, Ratnadewi D, Wungu TDK and Takemori H: Plant-derived exosome-like nanoparticles for biomedical applications and regenerative therapy. Biomedicines 11: 1053, 2023.
9. Sall IM and Flaviu TA: Plant and mammalian-derived extracellular vesicles: A new therapeutic approach for the future. Front Bioeng Biotechnol 11: 1215650, 2023.
10. Lian MQ, Chng WH, Liang J, Yeo HQ, Lee CK, Belaid M, Tollemeto M, Wacker MG, Czarny B and Pastorin G: Plant-derived extracellular vesicles: Recent advancements and current challenges on their use for biomedical applications. J Extracell Vesicles 11: e12283, 2022.
11. Ju S, Mu J, Dokland T, Zhuang X, Wang Q, Jiang H, Xiang X, Deng ZB, Wang B, Zhang L, *et al*: Grape exosome-like nanoparticles induce intestinal stem cells and protect mice from DSS-induced colitis. Mol Ther 21: 1345-1357, 2013.
12. Wang B, Zhuang X, Deng ZB, Jiang H, Mu J, Wang Q, Xiang X, Guo H, Zhang L, Dryden G, *et al*: Targeted drug delivery to intestinal macrophages by bioactive nanovesicles released from grapefruit. Mol Ther 22: 522-534, 2014.
13. Li DF, Tang Q, Yang MF, Xu HM, Zhu MZ, Zhang Y, Tian CM, Nie YQ, Wang JY, Liang YJ, *et al*: Plant-derived exosomal nanoparticles: Potential therapeutic for inflammatory bowel disease. Nanoscale Adv 5: 3575-3588, 2023.
14. Choi W, Cho JH, Park SH, Kim DS, Lee HP, Kim D, Kim HS, Kim JH and Cho JY: Ginseng root-derived exosome-like nanoparticles protect skin from UV irradiation and oxidative stress by suppressing activator protein-1 signaling and limiting the generation of reactive oxygen species. J Ginseng Res 48: 211-219, 2024.
15. Kim M, Jang H, Kim W, Kim D and Park JH: Therapeutic applications of plant-derived extracellular vesicles as antioxidants for oxidative stress-related diseases. Antioxidants (Basel) 12: 1286, 2023.
16. Morgan C and Nigam Y: Naturally derived factors and their role in the promotion of angiogenesis for the healing of chronic wounds. Angiogenesis 16: 493-502, 2013.
17. Roleira FM, Tavares-da-Silva EJ, Varela CL, Costa SC, Silva T, Garrido J and Borges F: Plant derived and dietary phenolic antioxidants: Anticancer properties. Food Chem 183: 235-258, 2015.
18. Cui X, Lin Q and Liang Y: Plant-derived antioxidants protect the nervous system from aging by inhibiting oxidative stress. Front Aging Neurosci 12: 209, 2020.
19. Hussain T, Jeena G, Pitakbut T, Vasilev N and Kayser O: Cannabis sativa research trends, challenges, and new-age perspectives. iScience 24: 103391, 2021.
20. Stasilowicz-Krzemien A, Sip S, Szulc P and Cielecka-Piontek J: Determining antioxidant activity of cannabis leaves extracts from different varieties-unveiling Nature's Treasure Trove. Antioxidants (Basel) 12: 1390, 2023.
21. Koltai H and Shalev N: Anti-Cancer activity of Cannabis Sativa Phytocannabinoids: Molecular mechanisms and potential in the fight against ovarian cancer and stem cells. Cancers (Basel) 14: 4299, 2022.
22. Zaiachuk M, Suryavanshi SV, Pryimak N, Kovalchuk I and Kovalchuk O: The anti-inflammatory effects of cannabis sativa extracts on LPS-induced cytokines release in human macrophages. Molecules 28: 4991, 2023.
23. Zagorska-Dziok M, Bujak T, Ziemlewska A and Niziol-Lukaszewska Z: Positive effect of Cannabis sativa L. Herb extracts on skin cells and assessment of Cannabinoid-Based Hydrogels properties. Molecules 26: 802, 2021.
24. Kim WS, Ha JH, Jeong SH, Lee JI, Lee BW, Jeong YJ, Kim CY, Park JY, Ryu YB, Kwon HJ and Lee I: Immunological effects of aster yomena callus-derived extracellular vesicles as potential therapeutic agents against allergic Asthma. Cells 11: 2805, 2022.
25. Lee HJ, Shin KW, Lee SJ, Park JY, Lee IC, Kwon HJ, Jeong HJ, Yuk JM, Ryu YB and Kim WS: Immunomodulation by extracellular vesicle-like nanoparticles from marine macroalgae Sargassum fusiforme: Enhancing type 1 T helper and cytotoxic T lymphocyte-mediated immune responses. J Funct Foods 112: 105981, 2024.
26. Livak KJ and Schmittgen TD. Analysis of relative gene expression data using real-time quantitative PCR and the 2(-Delta Delta C(T)) method. Methods 25: 402-408, 2001.
27. Blois MS: Antioxidant determinations by the use of a stable free radical. Nature 181: 1199-1200, 1958.
28. Re R, Pellegrini N, Proteggente A, Pannala A, Yang M and Rice-Evans C: Antioxidant activity applying an improved ABTS radical cation decolorization assay. Free Radic Biol Med 26: 1231-1237, 1999.
29. Ou X, Wang H, Tie H, Liao J, Luo Y, Huang W, Yu R, Song L and Zhu J: Novel plant-derived exosome-like nanovesicles from Catharanthus roseus: Preparation, characterization, and immunostimulatory effect via TNF-alpha/NF-kappaB/PU.1 axis. J Nanobiotechnology 21: 160, 2023.
30. Niu C and Aisa HA: Upregulation of melanogenesis and tyrosinase activity: Potential agents for Vitiligo. Molecules 22: 1303, 2017.
31. El-Nashar HAS, El-Din MIG, Hritcu L and Eldahshan OA: Insights on the inhibitory power of flavonoids on tyrosinase activity: A survey from 2016 to 2021. Molecules 26: 7546, 2021.
32. Lim JW, Ha JH, Jeong YJ and Park SN: Anti-melanogenesis effect of dehydroglyasperin C through the downregulation of MITF via the reduction of intracellular cAMP and acceleration of ERK activation in B16F1 melanoma cells. Pharmacol Rep 70: 930-935, 2018.
33. Cargnello M and Roux PP: Activation and function of the MAPKs and their substrates, the MAPK-activated protein kinases. Microbiol Mol Biol Rev 75: 50-83, 2011.
34. Jang JY, Lee JH, Kang BW, Chung KT, Choi YH and Choi BT: Dichloromethane fraction of Cimicifuga heracleifolia decreases the level of melanin synthesis by activating the ERK or AKT signaling pathway in B16F10 cells. Exp Dermatol 18: 232-237, 2009.
35. Emanuelli M, Sartini D, Molinelli E, Campagna R, Pozzi V, Salvolini E, Simonetti O, Campanati A and Offidani A: The double-edged sword of oxidative stress in skin damage and melanoma: From physiopathology to therapeutical approaches. Antioxidants (Basel) 11: 612, 2022.
36. Nakai K and Tsuruta D: What are reactive oxygen species, free radicals, and oxidative stress in skin diseases? Int J Mol Sci 22: 10799, 2021.

37. Ansary TM, Hossain MR, Kamiya K, Komine M and Ohtsuki M: Inflammatory molecules associated with ultraviolet radiation-mediated skin aging. Int J Mol Sci 22: 3974, 2021.
38. Kawakami A and Fisher DE: The master role of microphthalmia-associated transcription factor in melanocyte and melanoma biology. Lab Invest 97: 649-656, 2017.
39. Gelmi MC, Houtzagers LE, Strub T, Krossa I and Jager MJ: MITF in normal melanocytes, cutaneous and uveal melanoma: A delicate balance. Int J Mol Sci 23: 6001, 2022.
40. Ko GA and Cho SK: Phytol suppresses melanogenesis through proteasomal degradation of MITF via the ROS-ERK signaling pathway. Chem Biol Interact 286: 132-140, 2018.
41. Cheng ZJ, Dai GF, Hsu JL, Lin JJ, Wu WT, Su CC and Wu YJ: Antimelanogenesis effect of methyl gallate through the regulation of PI3K/Akt and MEK/ERK in B16F10 melanoma cells. Evid. Based Complement Alternat Med 2022: 5092655, 2022.
42. Chae JK, Subedi L, Jeong M, Park YU, Kim CY, Kim H and Kim SY: Gomisin N inhibits melanogenesis through regulating the PI3K/Akt and MAPK/ERK signaling pathways in Melanocytes. Int J Mol Sci 18: 471, 2017.
43. Song YC, Lee Y, Kim HM, Hyun MY, Lim YY, Song KY and Kim BJ: Berberine regulates melanin synthesis by activating PI3K/AKT, ERK and GSK3β in B16F10 melanoma cells. Int J Mol Med 35: 1011-1016, 2015.
44. Smejkal K, Slapetova T, Krmencik P, Babula P, Dall'Acqua S, Innocenti G, Vančo J, Casarin E, Carrara M, Kalvarová K, *et al*: Evaluation of cytotoxic activity of Schisandra Chinensis Lignans. Planta Med 76: 1672-1677, 2010.
45. Singh N and Sharma B: Toxicological effects of Berberine and Sanguinarine. Front Mol Biosci 5: 21, 2018.
46. Liu HM, Cheng MY, Xun MH, Zhao ZW, Zhang Y, Tang W, Cheng J, Ni J and Wang W: Possible mechanisms of oxidative stress-induced skin cellular senescence, inflammation, and cancer and the therapeutic potential of plant polyphenols. Int J Mol Sci 24: 3755, 2023.
47. Wei M, He X, Liu N and Deng H: Role of reactive oxygen species in ultraviolet-induced photodamage of the skin. Cell Div 19: 1, 2024.
48. Rodriguez-Casado A: The health potential of fruits and vegetables phytochemicals: Notable examples. Crit Rev Food Sci Nutr 56: 1097-1107, 2016.
49. Barbieri R, Coppo E, Marchese A, Daglia M, Sobarzo-Sánchez E, Nabavi SF and Nabavi SM: Phytochemicals for human disease: An update on plant-derived compounds antibacterial activity. Microbiol Res 196: 44-68, 2017.
50. Gonzalez-Vallinas M, Gonzalez-Castejon M, Rodriguez-Casado A and de Molina AR: Dietary phytochemicals in cancer prevention and therapy: A complementary approach with promising perspectives. Nutr Rev 71: 585-599, 2013.